Journal of Alloys and Compounds 512 (2012) 149–155

Contents lists available at SciVerse ScienceDirect

Journal of Alloys and Compounds

journal homepage: www.elsevier.com/locate/jallcom

Band gap and superior refractive index tailoring properties in nanocomposite thin film achieved through sol–gel co-deposition method

K. Joy*, S. Sujatha Lakshmy, Prabitha B. Nair, Georgi P. Daniel

Thin Film Lab, Research Department of Physics, Mar Ivanios College, Thiruvananthapuram 695015, India

ARTICLE INFO

Article history:
Received 6 June 2011
Received in revised form
17 September 2011
Accepted 19 September 2011
Available online 1 October 2011

Keywords:
Thin films
Sol–gel processes
Optical properties
X-ray diffraction
X-ray photoelectron spectroscopy
SEM

ABSTRACT

Transparent nanocomposite ZrO_2–SnO_2 thin films with molar ratio 0.1/0.9 (ZS19), 0.3/0.7 (ZS37), 0.5/0.5 (ZS55), 0.7/0.3 (ZS73) and 0.9/0.1 (ZS91) of ZrO_2/SnO_2 were prepared by sol–gel dip-coating technique. X-ray diffraction (XRD) spectra showed a mixture of three phases: tetragonal ZrO_2 and SnO_2 and orthorhombic $ZrSnO_4$. X-ray photoelectron spectroscopy (XPS) gives Zr 3d, Sn 3d and O1s spectra on ZS55 thin film which revealed the presence of oxygen vacancies in the nanocomposite ZrO_2–SnO_2 thin film. Scanning electron microscopy (SEM) observations showed that microstructure of ZS55 consists of uniformly dispersed isolated SnO_2 particles in ZrO_2 matrix. An average transmittance greater than 85% (in UV–visible region) is observed in the films ZS55, ZS73 and ZS91, but superior optical properties was observed in ZS55 thin film. The composite system under certain compositional mixings (ZS55) displayed a refractive index supremacy over pure zirconia films which can be directly employed in extending the range of tunability of the refractive index. Besides, these films also demonstrated tailoring of band gap values. Photoluminescence (PL) spectra revealed an intense emission peak at 424 nm in ZS55 sample which indicates the presence of oxygen vacancies in $ZrSnO_4$. All these characterizations distinctly indicate a strong interrelation between the microstructural ordering and superior optical properties of the present ZrO_2–SnO_2 co-deposited composites.

1. Introduction

Thin films of metal oxides have been of great interest because of their essential roles in electronic, electrical, optical and luminescence applications. Among these films, SnO_2 thin films have been studied intensively, since they have diverse applications in photovoltaic cells, solar energy collectors, optoelectronic devices, transparent conductors and gas sensors [1–5]. SnO_2 is a degenerate semiconductor with band gap energy (E_g) in the range of 3.4–4.6 eV [6,7]. This scatter in band gap energy (E_g) values of SnO_2 may be due to wide extent of non-stoichiometry of the deposited layers.

On the other hand, ZrO_2 is an important multifunctional transition metal oxide widely used in a variety of applications such as ceramics, oxygen and NOx sensors, solid oxide fuel cell electrolytes [8] and semiconductor devices. It is an ideal media for applications in photonics due to its excellent mechanical, electrical, thermal, optical, and stable photochemical properties [9]. It is an active and typical photon absorber among wide band gap (E_g) metal oxides with two interband transitions: an indirect transition at 5.22 eV followed by a direct transition at 5.87 eV [10,11]. Pure zirconia has three solid polymorphs which exhibit monoclinic, tetragonal and cubic symmetries. The use of pure zirconia ceramics as advanced structural materials is limited due to the spontaneous tetragonal to monoclinic ($t \rightarrow m$) phase transformation upon cooling from elaboration temperature to room temperature. This martensitic transition results in irreversible damages caused by about 4.5% volume expansion [12,13].

The synthesis of advanced optical materials endowed with enhanced physical and mechanical properties has progressively focused on composite systems which can involve complex stoichiometry and/or microstructures [14–16]. Tailoring of refractive index along with dense microstructure are the demanding requirements in the development of precision and high-end optical coatings.

There has been a continuous striving to improve upon the packing density by adopting process optimization techniques [17]. It is seen that an oxide thin film can be stabilized by adding a certain amount of different (foreign) oxide [12,18,19]. Štefanić and Musić reported the stabilization of tetragonal polymorph of ZrO_2 by incorporation of suitable trivalent cations [18]. Štefanić et al. found that incorporation of tetravalent dopants could partially stabilize the tetragonal polymorph of zirconia [19]. Such a technique can be realized by co-deposition technique [19,20]. This has several favourable outcomes where it is possible to achieve optical and microstructural tunabilities between the properties of the two or more participating components. Such mixed-composition

* Corresponding author. Tel.: +91 471 2531053; fax: +91 471 2530023.
E-mail address: jolly2jolly@gmail.com (K. Joy).

0925-8388/$ – see front matter © 2011 Elsevier B.V. All rights reserved.
doi:10.1016/j.jallcom.2011.09.051

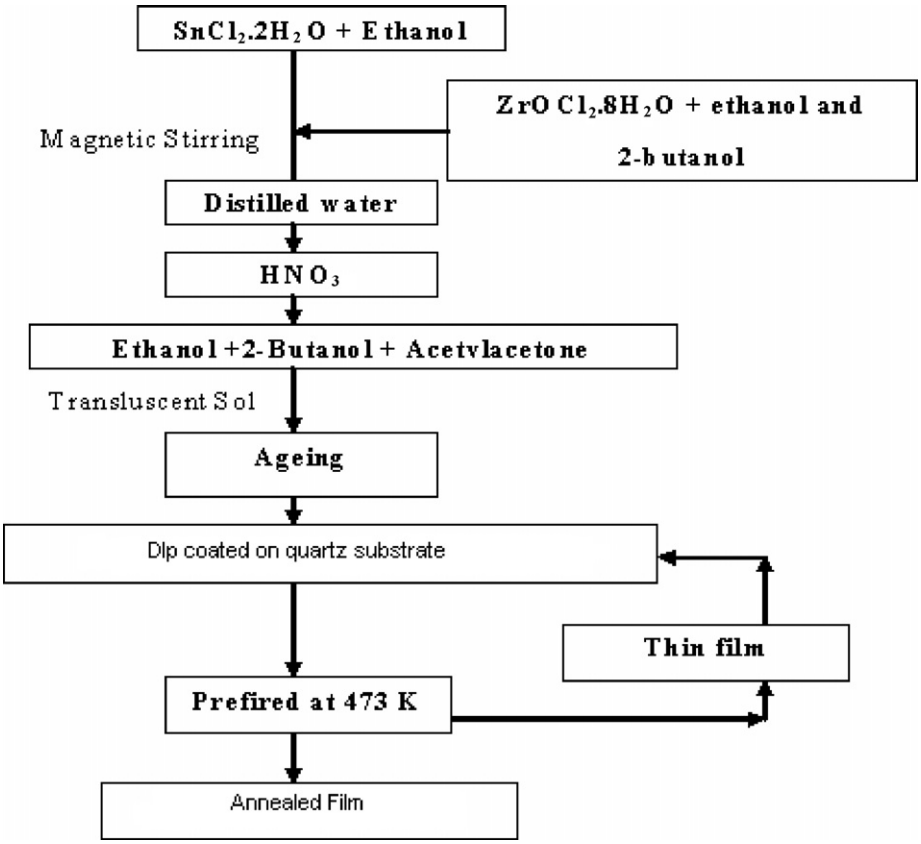

Fig. 1. Flowchart of preparation of nanocomposite ZrO_2–SnO_2 thin films by sol–gel method.

systems often exhibit improved optical and physical properties against the participating component films [21–23]. The prime interest in such mixed nanocomposite systems relies on the possibilities to tailor the optical and electrical properties over a wide range of values [24,25]. To tailor the properties of these nanocomposites and to make them suitable for practical application, the understanding of their microsructural aspect is foremost important.

The presently studied ZrO_2–SnO_2 nanocomposite film has depicted several such novel properties which have distinct advantages both with respect to the tunability in the optical properties as well as in superior microstructure that controls the band gap favourably for applications in optical and gas sensing devices [8,26]. It was particularly noticed that by admixing SnO_2 in ZrO_2 under certain compositional ratios the optical properties such as refractive index, energy gap and photoluminescence properties are dominantly influenced by the microstructure than the stoichiometry. Photoluminescence studies provide information about a material on electronic band transitions, structure and defects. In the case of thin films, surfaces play particularly important role. Surface states formed by surface defects (e.g. ion vacancies, surface ions with low coordination numbers, and groups coordinated on the surface of materials) introduce localized energy levels within the forbidden gap. These mid-gap surface states are expected to become luminescence centers under an appropriate excitation [27].

Sol–gel coating techniques have proved to be a popular means of fabricating nanocomposite thin films in the nanometer thickness range [28,29] The basis of this technique is to coat a substrate with a precursor solution containing the requisite metal components in the required proportion, which then, because of solvent evaporation and/or chemical reactions, transforms to a gel layer. The organic components of the gel are then eliminated by various heat treatments to form the desired crystalline thin film. Since sol gel method is a solution process, it has the advantages of purity, homogeneity, felicity and flexibility in introducing dopants in large concentrations, stoichiometric control, ease of processing and composition control [30]. The main advantage of the sol–gel process is the ability to form inorganic structures at relatively low temperature. Moreover, the process is a cost-effective way to produce thin homogeneous inorganic films on large scales.

There are several investigations related to the ZrO_2–SnO_2 system. Hunter et al. [31] and Kim et al. [32] investigated the influence of Sn^{4+} ions incorporation into the tetragonal ZrO_2–2 mol% Y_2O_3 system. Hunter et al. and Kim et al. found that the replacement of Zr^{4+} ions with smaller Sn^{4+} ions caused an increase in the unit-cell volume of t-ZrO_2. However, the presence of tin could not suppress the transition to a monoclinic ZrO_2 after cooling to room temperature. Dhage et al. [33] reported a solubility of Sn^{4+} ions in the m-ZrO2 lattice (20 mol%) occurred in the product obtained upon 15 h of calcination at 1000 °C. Štefanić et al. [19] found that the incorporation of Sn^{4+} ions caused an asymmetric distortion of monoclinic ZrO_2 lattice. However, the unit cell volume of monoclinic ZrO_2 remained unchanged almost. They also reported the appearance of a metastable $ZrSnO_4$ phase, in products having 40 or 50 mol% of SnO_2 calcined at 1000 °C. In spite of these attempts, so far there are no authentic studies on the superior optical and photoluminescence properties of ZrO_2–SnO_2 composite thin films. In our study we, however, noticed a prominent microstructural ordering that led to superior optical and photoluminescence properties. Besides, XPS studies revealed the chemical composition, chemical state of the surface

species and different defect states in the ZrO_2–SnO_2 composite thin film.

2. Experimental details

ZrO_2–SnO_2 precursor solutions with different molar ratios (0.1/0.9, 0.3/0.7, 0.5/0.5, 0.7/0.3 and 0.9/0.1 of ZrO_2/SnO_2) were prepared. In the typical preparation one set each of 0.9, 0.7, 0.5, 0.3 and 0.1 mol of $SnCl_2 2H_2O$ (tin(II) chloride dihydrate) dissolved in appropriate amount of ethanol (1 mol/l) was taken and each batch was stirred well for 3 h. Then, 0.1, 0.3, 0.5, 0.7 and 0.9 mol each of $ZrOCl_2 8H_2O$ (zirconium oxychloride octahydrate) (Sigma–Aldrich 99.5%) dissolved in one third part of a solution of 2-butanol and ethanol taken in 1:1 ratio, were also taken, followed by stirring for 45 min using a magnetic stirrer. The solution containing the precursor of SnO_2 was then carefully added in the respective batch of zirconium oxychloride octahydrate–alcohol solution under vigorous stirring. Subsequently, the water for hydrolysis, the nitric acid for oxidation and the remaining part of the 2-butanol–ethanol mixture, with required amount of acetyl-acetone, were added under vigorous stirring in a controlled manner. The stirring was continued for 90 min until a clear transparent sol is obtained. Zirconium oxychloride octahydrate, water, nitric acid and acetyl-acetone were taken in the molar ratio 1:20:0.4:3 [34]. Fig. 1 shows the flowchart for the synthesis of nanocomposite ZrO_2–SnO_2 thin film [35]. The filtered precursor solution was deposited on clean quartz substrates using an indigenously fabricated dip coating apparatus. The dip coating parameters were optimized as 10 cm/min lifting speed and 90° vertical lifting, depending on the viscosity and concentration of the precursor solution. The dip coated films were dried at room temperature and prefired at 150 °C for 1 h. The process of dipping and prefiring was repeated five times as five coatings were required to obtain useful data from X-ray diffraction characterization. Next the samples were heated up to 500 °C at a heating rate of 4 °C/min, and held at this temperature for 1 h and finally cooled to room temperature at the same rate. The nanocomposite ZrO_2–SnO_2 thin films with molar ratio 0.1/0.9 (ZS19), 0.3/0.7 (ZS37), 0.5/0.5 (ZS55), 0.7/0.3 (ZS73) and 0.9/0.1 (ZS91) of ZrO_2/SnO_2 were also prepared in a similar way. The structural and optical characterizations of these annealed films were then performed.

Crystallization phase of the nanocomposite thin film was characterized by X-ray diffractometer (XRD) (Bruker-AXS-D8 Advance XRD). XPS spectrum was recorded using a monochromatic Al Kα (1486.6 eV) source and a MAC-2 electron analyzer (RIBER system model-FCX 700). Surface morphology of the film was investigated by scanning electron microscopy (JEOL Model JSM-6390LV). Optical transmittance was studied using a Spectrophotometer (Model – JASCO-V550). PL spectrum was recorded using a Perkin-Elmer Fluorescence Spectrometer (Model – LS55) with a 40 W Xenon Lamp as the excitation source and 3 nm excitation and emission slit width.

3. Results and discussion

3.1. X-ray diffraction studies

The X-ray diffraction spectra of the nancomposite ZrO_2–SnO_2 films (ZS19, ZS37, ZS55, ZS73 and ZS91) deposited on quartz substrates annealed at 500 °C are shown in Fig. 2. The spectra show that the films ZS19, ZS37, ZS73 and ZS91 are polycrystalline with characteristic peaks of tetragonal ZrO_2 (t-ZrO2) phase at $2\theta = 30.2°$, 35.4°, 50.3°, 60.2° [PDF No. 79-1769] and tetragonal SnO_2 phase at $2\theta = 26.5°$, 33.7°, 51.8° [PDF No. 88-0287], respectively. Štefanić et al. [19] has reported that metastable $ZrSnO_4$ phase appears only in systems calcined at 1000 °C or at higher temperatures. However, in our study, ZS55 sample with molar ratio 0.5/0.5 of ZrO_2/SnO_2 shows the growth of orthorhombic $ZrSnO_4$ phase at $2\theta = 51.7°$ and 62.7° [PDF No. 48-0889] along with tetragonal ZrO_2 and tetragonal SnO_2 phase on films annealed at 500 °C. The formation of $ZrSnO_4$ in the ZS55 film is due to the maximum solubility of Sn^{4+} ions in the ZrO_2 lattice when prepared in the molar ratio 0.5:0.5 occurred in the products obtained upon crystallization. Table 1 summarizes the composition, 2θ angles of (1 1 1) peak of t-ZrO_2 and phase composition of the samples.

In our earlier studies, we have observed that pure zirconia thin films attain a mixed tetragonal and monoclinic (m) crystalline phases at an annealing temperature of 500 °C [34]. The results of the present study shows the presence of stabilized tetragonal ZrO_2 (t-ZrO_2) polymorph in ZS91, ZS73, ZS55 and ZS73 samples annealed at 500 °C. These crystallization products probably results from a ZrO_2–SnO_2 surface interaction, similarly as in the ZrO_2/SO_4^{2-} system [36] that prevents the diffusion

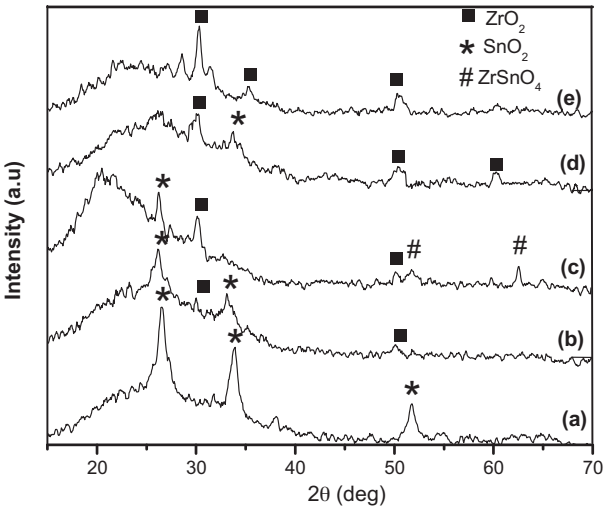

Fig. 2. XRD pattern of nanocomposite ZrO_2–SnO_2 thin films: (a) ZS91, (b) ZS37, (c) ZS55, (d) ZS73 and (e) ZS91 deposited on quartz annealed at 500 °C.

of oxygen from the atmosphere into the ZrO_2 lattice and triggers the t-ZrO_2 to m-ZrO_2 transition. The surface interaction appeared to be a very important factor in stabilization of the t-ZrO_2 type phase in the crystallization products of ZrO_2–SnO_2 systems.

A closer look at the diffraction patterns of crystallization products annealed at 500 °C, containing the most prominent diffraction lines of t-ZrO_2, shows that an increase in SnO_2 content shifts the diffraction lines of t-ZrO_2 phases to a lower angle (Table 1). This indicates that incorporation of Sn^{4+} ions causes an asymmetric distortion of the t-ZrO_2 lattice which would produce a change in the stress of the ZrO_2–SnO_2 systems. However, trace amount of SnO_2 may be segregated at the surface of the films which might influence the low energy photoluminescence peaks originating from the surface states.

3.2. XPS studies

Fig. 3 shows XPS core level spectra of ZS55 film sample annealed at 500 °C. The peaks denoted by solid curves are calibrated with respect to the C1s peak position set at 285.1 eV. It gives information about the changes in the electronic states of Zr, Sn and O atoms in ZrO_2–SnO_2 nanocomposite. For each line the best fit is also drawn, taking into account a Gaussian shape. The doublets of Zr $3d_{5/2}$ and Zr $3d_{3/2}$ levels were measured at 180.9 and 184.6 eV, respectively [37]. The calibrated energy scale assigns the O1s peak with the BE ~530 eV to the $O2^-$ species in the compounds. The small shoulder at 530.7 eV is assigned to lattice oxygen while the main peak at 532.6 eV may be attributed to oxygen in adsorbed hydroxyl groups. The existence of multipeaks (530.7 and 532.6 eV) is related to the presence of oxygen defects [38]. The Sn $3d_{5/2}$ located at about 486.4 eV, demonstrates that the chemical state of Sn in the sample is +4. The peak at about 496 eV is Sn $3d_{3/2}$ level [39].

Zhou et al. [40] has observed that oxygen vacancies and tin interstitials have low formation energies and these defects of high concentrations can easily exist and act as long range carriers. The SnO_2 phase can accommodate a significant amount of oxygen vacancies as reported by Li Zi et al. [41]. The quantitative analysis was done from the normalized areas of the Zr 3d/O1s and Sn 3d/O1s peaks which shows a molar ratio of O/Zr ~ 1.65 and

Table 1
Composition, diffraction angle and phase composition of nanocomposite ZrO_2–SnO_2 thin films on quartz annealed at 500 °C.

Sample	ZrO_2 (mol)	SnO_2 (mol)	Diffraction angle 2θ (°)	Phase composition		
ZS19	0.1	0.9	–	–	SnO_2	–
ZS37	0.3	0.7	30.05	ZrO_2	SnO_2	–
ZS55	0.5	0.5	30.15	ZrO_2	SnO_2	$ZrSnO_4$
ZS73	0.7	0.3	30.21	ZrO_2	SnO_2	–
ZS91	0.9	0.1	30.32	ZrO_2	–	–

O/Sn ~ 1.72, which is smaller than the value for stoichiometric ZrO_2 and SnO_2, suggesting the presence of oxygen vacancies [42]. This oxygen vacancy contributes to the PL in nanocomposite ZrO_2–SnO_2 thin film.

3.3. Microstructural studies

Fig. 4 shows the scanning electron micrograph of nanocomposite ZrO_2–SnO_2 thin films ZS19, ZS37, ZS55, ZS73 and ZS91 on quartz annealed at 500 °C. By adding ZrO_2, two phenomena, in principle, could be acting. One is the interconnection between original SnO_2 grains by ZrO_2 phase. The other is the simultaneous filling of SnO_2 pores. These two effects lead, firstly, to an aggregation of the resultant composite particles. By thermal treatment at 500 °C, and considering the differences in molar ratios of films, these two effects produce small aggregates seen in ZS19 and ZS37. By increasing the amount of ZrO_2 the microstructure of the composite ZS55 becomes more uniform. For 0.5/0.5 ratio (ZrO_2/SnO_2) homogeneous dispersion of isolated SnO_2 particles in ZrO2 matrix is observed. Further increasing of the ZrO_2 phase contents, hardly any SnO_2 particles can be seen dispersed in ZrO_2 matrix (ZS73 image) and results in the film cracking, as is evident in the ZS91 image.

3.4. Optical studies

Fig. 5 shows the spectral transmittance of nanocomposite ZrO_2–SnO_2 thin films (various molar ratios) on quartz annealed at 500 °C. The presence of oscillations in the composite thin films is indicative of the homogeneity and uniform thickness of the film. It can be noticed from the spectra that ZS55 film has demonstrated superior spectral profiles. In this molar ratio, SnO_2 is found to be highly dispersed in ZrO_2 matrix (SEM image ZS55). However, excessive SnO_2 could not disperse uniformly due to the phase separation caused by the aggregation of excessive SnO_2 (SEM images ZS37 and ZS19). A proper amount of SnO_2 could improve the optical transmittance of the nanocomposite film due to the synergic effect between SnO_2 and ZrO_2. However excessive SnO_2 led to the phase separation which decreased the transmittance of the nanocomposite ZrO_2–SnO_2 thin films. At the absorption edge, the interference fringes gradually disappeared, and all spectra show a sharp fall of transmittance derived from the fundamental absorption of the films. Furthermore, with increasing molar ratio of ZrO_2/SnO_2, a clear blue shift of these interference free regions can be observed suggesting a remarkable increase in the band gap of the films. Optical band gap (E_g) values are obtained by extrapolating the linear portion of $(\alpha h\upsilon)^2$ versus $h\upsilon$ plots [Fig. 5 inset] to intercept the photon energy axis [43].

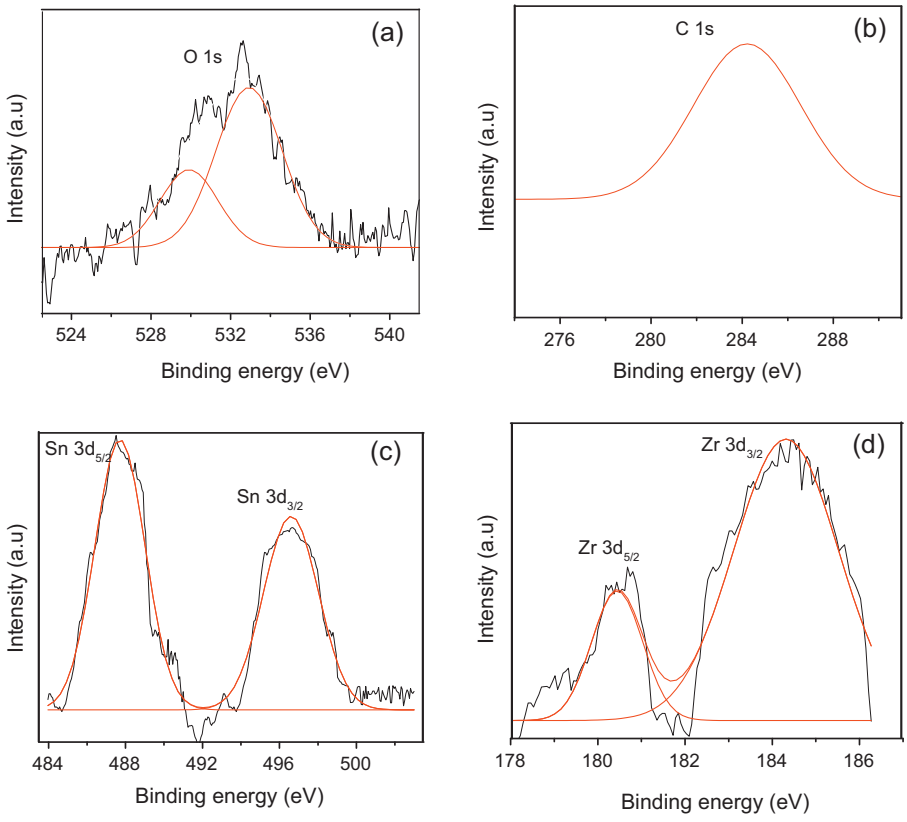

Fig. 3. XPS spectra of nanocomposite ZrO_2–SnO_2 thin film ZS55 annealed at 500 °C: (a) O1s, (b) C1s, (c) Sn 3d and (d) Zr 3d.

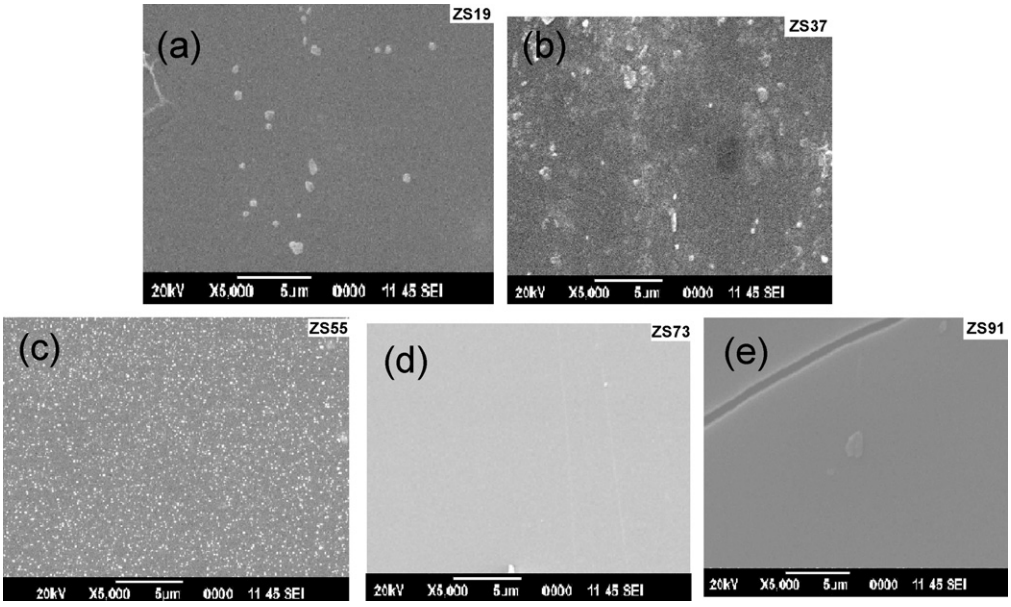

Fig. 4. SEM micrograph of nanocomposite ZrO_2–SnO_2 thin films: (a) ZS19, (b) ZS37, (c) ZS55, (d) ZS73 and (e) ZS91 on quartz annealed at 500 °C.

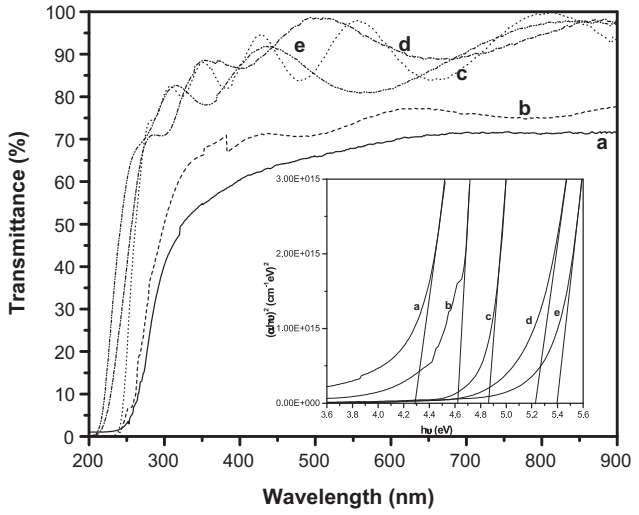

Fig. 5. Transmission spectra of nanocomposite ZrO_2–SnO_2 thin films: (a) ZS91, (b) ZS37, (c) ZS55, (d) ZS73 and (e) ZS91 deposited on quartz annealed at 500 °C. Inset shows plots of $(\alpha h\nu)^2$ versus $h\nu$ curve.

Table 2 gives the thickness, band gap and refractive index of the composite thin films which are calculated from the Swanepoel's method [43] .The refractive indices values show composite dependent evolution of the refractive index of the composite films. The ZS55 sample shows higher value of refractive index with respect to nanocomposite films of other molar ratios (Table 2) and sol–gel derived pure zirconia films [44]. This may be due to better densification of the ZS55 composite thin film. We can infer that the ZS55 composite film has a better crystallinity than the other Zr:Sn ratio films. The band gap of the nanocomposite thin film decreases from 5.58 to 4.28 eV with increase in Sn concentration. The change in the band gap is realized by incorporating the molecular structure of SnO_2 into the solid net works of the ZrO_2 thin films.

Table 2
Thickness, band gap and refractive index of nanocomposite ZrO_2–SnO_2 thin films on quartz annealed at 500 °C.

Sample	Thickness (nm)	Band gap (eV)	Refractive index (n)
ZS19	–	4.28	–
ZS37	182	4.78	1.79
ZS55	302	4.97	2.11
ZS73	182	5.43	1.95
ZS91	229	5.58	1.92

At this point, it should be noticed that the band gap value can be easily tuned by simply changing the relative concentration of zirconium and tin elements. The most interesting aspect noticed in the present experiment is the superior spectral refractive index feature of ZS55 composite film over other molar ratio and pure zirconia films. Such a condition can favourably be utilized in the tuning of the refractive index and band gap beyond the values of the participating components.

3.5. Photoluminescence

The selective emission and absorption of specific frequencies can be connected to the presence of impurities (foreign elements) and imperfections that provide localized energy levels in the forbidden energy gap. Luminescent materials generally contain impurities called activators, which contribute to energy levels, which are responsible for the emission of visible light. Precursors based on Zr and Sn contain small percentage of intrinsic impurities that contributed to surface defects formation (Zr interstitials, Sn interstitials). However, it does not cause the main effect of luminescence. An effective activator level is that level which the electron finds it easy to enter and leave. Otherwise the electron may prefer to recombine directly, by descending to the valence band. There are two possibilities of recombination taking place: (a) the electron descends to an excited activator level, and radiates by a transition to the activator ground state and (b) the electron is first trapped in levels that do not allow transitions involving radiation. The electron is eventually excited to the conduction band and then radiated by going to an activator level.

According to the excitation spectra of all samples (not shown here), the absorption intensities of ZrO_2 and SnO_2 particles are very weak, where as the nanocomposite thin film shows a strong absorption at 373 nm. It is well known that, the high PL efficiency is based on the intense absorption of excitation light, so it can be believed that the nanocomposite material gives much more intense photoluminescence at the excitation wavelength 373 nm. The emission

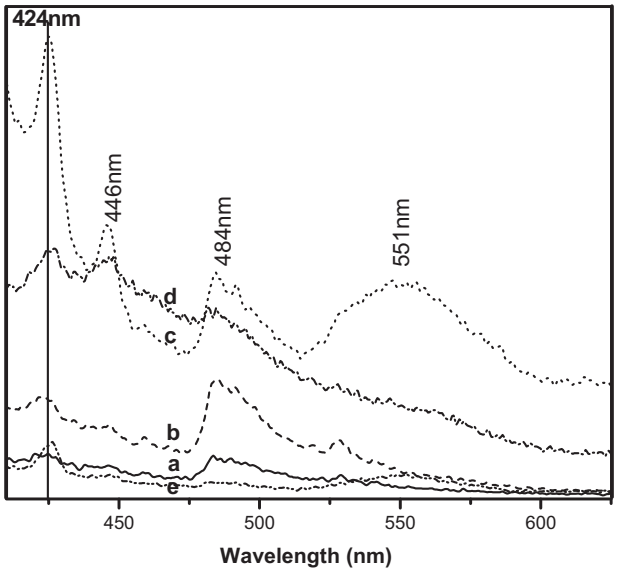

Fig. 6. PL spectra of nanocomposite ZrO_2–SnO_2 thin films: (a) ZS91, (b) ZS37, (c) ZS55, (d) ZS73 and (e) ZS91 deposited on quartz annealed at 500 °C excited at 373 nm.

spectra of the samples annealed at 500 °C are shown in Fig. 6. The emission spectrum for ZS55 consists of emission peaks at 424, 446, 484 and a broad peak centered at 551 nm.

The emission peak at 424 nm may be due to oxygen vacancies in $ZrSnO_4$ which interact with interstitial atoms of zirconium and tin and lead to the formation of trapped states within the band gap giving rise to photoluminescence [45]. The blue PL emission peak observed at 446 nm is ascribed to the mid gap trap states of SnO_2 [46]. The peak at 484 nm is synonymous with the shoulder peak observed by Gao and Song in ZrO_2 at room temperature [47]. Soares et al. reported a broad emission band at 551 nm due to stabilized zirconia single crystals [48].

Because Sn or/and Zr in $ZrSnO_4$ is in orthorhombic oxygen coordination, the emission of the composite nanocrystals is also attributed to the similar surface defects in oxygen orthorhombohedron. Incorporating Zr^{4+} ions into SnO_2 creates different environment for oxygen atoms and then influence the environment of the surface defects, therefore the emission spectra of the nanocrystals doped with Zr^{4+} ions increased compared with that of pure nanocrystals. In addition, the Zr^{4+} ions can increase the disorder of the oxygen orthorhombohedron, and thus the PL intensity increases till ZS55. It is observed that further increase of Zr^{4+} content can weaken the emission as reported by Liu et al. [49]. So, the PL intensity of ZS73 is lower than that of ZS55.

It is well known that the photoluminescence depends strongly on the concentration of the activators. The PL intensity becomes weaker when the activators become more concentrated. This means the more the SnO_2 particles uniformly dispersed, the more the luminescence is efficient. From the above results, it is clear that, the SnO_2 particles are adsorbed on the surface of ZrO_2 particles, so the interaction between the SnO_2 particles decreases and a good dispersion of SnO_2 particles is obtained (SEM image of ZS55) and as a result, the peak at 446 nm of the nanocomposite ZS55 shows an increase in the PL intensity. On the other hand, if too many SnO_2 particles are adsorbed on the surface of ZrO_2 particles, they will combine with each other and aggregates will be formed (SEM images ZS19 and ZS37). As a result the energy band gap of the nanocomposite decreases and the interaction between electrons and phonon increases [50], and this phenomenon directly caused a red shift of the peak wavelength and a decrease of the PL intensity.

4. Conclusions

The presently studied composite ZrO_2–SnO_2 thin films deposited through sol–gel co-deposition process have demonstrated several interesting optical, microstructural and morphological evolutions. The addition of certain amount of SnO_2 in ZrO_2 has resulted in densification of microstructure and the formation of orthorhombic $ZrSnO_4$ phase in the film annealed at 500 °C. This has also resulted in a better grain structure ordering which ultimately led to display of superior spectral refractive index profiles and enhanced PL emission. Besides these films also demonstrated the tailoring of band gap values. The PL emission peak of the composite film at 424 nm excited at an excitation wavelength of 373 nm indicates the presence of oxygen vacancies which interact with interfacial atoms of zirconium and tin giving rise to photoluminescence. These composite films have opened up a new dimension in optical applications in which it is possible to tailor the band gap and refractive index in co-deposition process beyond the limits of the participating components.

Acknowledgement

The authors are grateful for the financial assistance of KSCSTE, Govt. of Kerala, India, Major Research Project (2009–2012).

References

[1] F. Gu, S. Wang, H. Cao, C. Li, Nanotechnology 19 (2008) 095708.
[2] S. Peng, F. Cheng, J. Liang, Z. Tao, J. Chen, J. Alloys Compd. 481 (2009) 786.
[3] A.A. Yadav, E.U. Masumdar, A.V. Moholkar, M. Neumann-Spallart, K.Y. Rajpure, C.H. Bhosale, J. Alloys Compd. 488 (2009) 350–355.
[4] C.D. Lokhande, P.M. Gondkar, R.S. Mane, V.R. Shinde, S.H. Han, J. Alloys Compd. 475 (2009) 304.
[5] G. He, G. Bhat, Z.W. Chen, J. Alloys Compd. (2011), doi:10.1016/j.jallcom.2011.07.053.
[6] A.E. Rakshani, Y. Makdisi, H.A. Ramazanyan, J. Appl. Phys. 83 (1998) 1049.
[7] S. Saipriya, R. Singh, J. Alloys Compd. (2011), doi:10.1016/j.jallcom.2011.07.019.
[8] G. Korotcenkov, Mater. Sci. Eng. R 61 (2008) 1–39.
[9] Y. Sorek, M. Zevin, R. Reisfeld, Chem. Mater. 9 (1997) 670.
[10] C.R. Aita, E.E. Hoppe, R.S. Sorbello, Appl. Phys. Lett. 82 (2003) 677.
[11] Q. Li, B. Chen, S. Xu, H. Gao, L. Zhang, C. Liu, J. Alloys Compd. 478 (2009) 544–549.
[12] C. Viazzi, J.-P. Bonino, F. Ansart, A. Barnab, J. Alloys Compd. 452 (2008) 377–383.
[13] A.M. Torres-Huerta, J.R. Vargas-García, M.A. Domínguez-Crespo, J.A. Romero-Serrano, J. Alloys Compd. 483 (2009) 394–398.
[14] L. Armelao, C. Eiesenmenger-Sittner, M. Groenewolt, S. Gross, C. Sada, U. Schubert, E. Tondello, A. Zattin, J. Mater. Chem. 15 (2005) 1838.
[15] K. Tahmasebi, M.H. Paydar, J. Alloys Compd. 509 (2011) 1192.
[16] R. Wongmaneerunga, S. Choopan, R. Yimnirun, S. Ananta, J. Alloys Compd. 509 (2011) 3547.
[17] D. Zhang, S. Fan, Y. Zhao, W. Gao, J. Shao, R. Fan, Y. Wang, Z. Fan, Appl. Surf. Sci. 243 (2005) 232.
[18] G. Štefanić, S. Musić, J. Alloys Compd. 460 (2008) 444.
[19] G. Štefanić, S. Musić, M. Ivanda, Mater. Res. Bull. 43 (2008) 2855.
[20] N.K. Sahoo, A.P. Shapiro, Appl. Opt. 37 (1998) 698.
[21] Y. Tsou, F.C. Ho, Appl. Opt. 35 (1996) 5091.
[22] S. Madhusudan, M.M.M. Sarcar, N.R.M.R. Bhargava, J. Alloys Compd. 471 (2009) 116.
[23] S.-N. Chou, J.-L. Huanga, D.-F. Lii, H.-H. Lu, J. Alloys Compd. 436 (2007) 124.
[24] J.S. Chen, S. Chao, J.S. Kao, H. Niu, C.H. Chen, Appl. Opt. 35 (1996) 90.
[25] B. Deb, A. Ghosh, J. Alloys Compd. 509 (2011) 2256.
[26] G. Korotcenkov, Sens. Actuators B 107 (1) (2005) 209–232.
[27] A.V. Emeline, G.V. kataeva, A.S. Litke, A.V. Rudakova, V.K. Ryabchuk, N. Serpone, Langmuir 14 (1998) 5011.
[28] N. Sriprang, D. Kaewchina, J.D. Kennedy, S.J. Milne, J. Am. Ceram. Soc. 83 (8) (2000) 1914.
[29] W. Shanga, B. Chen, X. Shi, Y. Chen, X. Xiao, J. Alloys Compd. 474 (2009) 541.
[30] M.A. Ahmed, M.F. Abdel-Messih, J. Alloys Compd. 509 (2011) 2154.
[31] B.A. Hunter, C.J. Howard, D.-J. Kim, J. Solid State Chem. 146 (1999) 363–368.
[32] D.J. Kim, J.W. Jang, H.L. Lee, J. Am. Ceram. Soc. 80 (1997) 1453–1461.
[33] S.R. Dhage, V. Samuel, R. Pasricha, V. Ravi, Ceram. Int. 32 (2006) 939.
[34] I. John Berlin, J.S. Lakshmi, S. Sujatha Lekshmy, P. Georgi Daniel, P.V. Thomas, K. Joy, J Sol–Gel Sci. Technol. 58 (3) (2011) 669, doi:10.1007/s10971-011-2443-6.
[35] J.S. Lakshmi, I. John Berlin, K. Jijimon Thomas, P.V. Thomas, K. Joy, IOP Conf. Ser.: Mater. Sci. Eng. 23 (2011), 012030.
[36] R. Srinivasan, T.R. Watkins, C.R. Hubbard, B.H. Davis, Chem. Mater. 7 (1995) 725–730.
[37] G. Cabello, L. Lillo, C. Caro, G.E. Buono-core, B. Cornik, M.A. Soto, J. Non-Cryst. Solids 354 (2008) 3919–3928.

[38] J.S. Lakshmi, I. John Berlin, P. Georgi Daniel, P.V. Thomas, K. Joy, Physica B 406 (2011) 3050–3055, doi:10.1016/j.physb.2011.05.004.
[39] F. Davar, M. Salavati-Niasari, Z. Fereshteh, J. Alloys Compd. 496 (2010) 638–643.
[40] J.X. Zhou, M.S. Zhang, J.M. Hong, Z. Yin, Solid State Commun. 138 (2006) 242–246.
[41] Y. Li Zi, S. Zhi-Thong, W. Chan-Zheng, J. Solid State Chem. 113 (1994) 221.
[42] A.S. Foster, V.B. Sulimov, F. Lopez Gejo, A.L. Schluger, R.M. Nieminen, Phys. Rev. B 64 (2001) 224108.
[43] R. Swanepoel, J. Phys. E: Sci. Instrum. 16 (1983) 1214.
[44] G. Ehrhart, B. Capoen, O. Robbe, Ph. Boy, S. Turrel, M. Bouazaoui, Thin Solid Films 496 (2006) 227.
[45] D. Sakar, D. Mohapatra, S. Ray, S. Bhattacharyya, S. Adak, N. Mitra, J. Mater. Sci. 42 (2007) 1847.
[46] F. Ji, J. Ma, Y.H. Wang, H.-L. Ma, X. Yu, F. Zong, Mater. Sci. Forum. 475–479 (2005) 3701.
[47] L. Gao, X.-Q. Song, J. Chin. Chem. Soc. 56 (2009) 310–313.
[48] M.R.N. Soares, C. Nico, M. Peres, N. Ferreira, A.J.S. Fernandes, T. Monteiro, F.M. Costa, J. Appl. Phys. 109 (2011) 013516, doi:10.1063/1.3527914.
[49] S.W. Liu, C.F. Song, M.K. Lü, F. Gu, S.F. Wang, D. Xu, D.R. Yuan, C.W. Wang, Mater. Sci. Eng. B104 (2003) 49–53.
[50] K. Hashmato, M. Hiramoto, T. Sakata, Chem. Phys. Lett. 148 (1988) 215.